# Examining fine potential energy effects in high-energy fission dynamics

K. Mazurek,[1,*] C. Schmitt,[2] P. N. Nadtochy,[3] M. Kmiecik,[1] A. Maj,[1] P. Wasiak,[1] and J. P. Wieleczko[2]
[1]*The Niewodniczański Institute of Nuclear Physics-PAN, 31-342 Kraków, Poland*
[2]*Grand Accélérateur National d'Ions Lourds, CEA/DSM-CNRS/IN2P3, 14076 Caen, France*
[3]*Omsk State University, Department of Theoretical Physics, 644077 Omsk, Russia*
(Received 26 June 2013; revised manuscript received 30 September 2013; published 19 November 2013)

The potential energy surface plays a decisive role in nuclear fission. Together with inertia and viscosity, it influences the trajectory of the system, and the properties of the fission fragments result from the puzzling interplay between static and dynamical effects. A careful study on the influence of the parametrization of the potential energy landscape in heavy-ion-induced fission is performed. Dynamical calculations are done within the stochastic Langevin approach in a three-dimensional deformation space. Various prescriptions of the potential energy surface are considered, probing two different Liquid Drop models and the deformation dependence of the Wigner/congruence energy. A wide set of observables, including cross sections, particle multiplicities, and integral, as well as isotopic and isobaric, distributions of fission and evaporation products, is analyzed. Nuclei close to the Businaro-Gallone point are confirmed to be well suited for investigating the Liquid Drop parametrization, while the influence of the deformation-dependent Wigner/congruence energy is difficult to demonstrate unambiguously in fission at high excitation energies.

DOI: 10.1103/PhysRevC.88.054614 PACS number(s): 25.70.Jj, 24.75.+i, 25.85.−w, 47.55.D−

## I. INTRODUCTION

A number of key nuclear structure properties and the dynamics of nuclear reactions critically depend on the potential energy of the system. Interpretation of experimental data thus relies on the prescription used for modeling the topography of the potential energy surface (PES). The latter defines the evolution of the energy of the nucleus as a function of its shape. It is crucial for the characterization of ground-state masses, the occurrence of shape coexistence and shape isomerism, and the path to various decays, including cluster radioactivity and spontaneous and induced fission. The description of these features requires several deformation degrees of freedom to be introduced to parametrize all relevant nuclear shapes. Two main approaches are used to calculate multidimensional PES. Microscopic self-consistent methods within the Hartree-Fock approach [1–3] are based on nucleon wave functions, automatically accounting for various features. Yet, such calculations become very demanding from a computational point of view, with an increase of the number of dimensions. In the alternative phenomenological macroscopic-microscopic approach (see Ref. [4] and therein), the PES is split into two parts: the sum of shape-dependent macroscopic and microscopic terms. The former contribution is computed within the Liquid Drop (LD) formalism [5,6], while the latter is commonly derived following the method proposed by Strutinsky [7]. Although self-consistent approaches may be considered to be based on a more fundamental level, macroscopic-microscopic models are numerically less involved and very flexible [8,9]. The macroscopic-microscopic method has been shown to be well suited for addressing various structural and dynamical aspects, among which are shape coexistence in medium-mass nuclei [8], hyperdeformation [10], stability of superheavy nuclei [11], and giant dipole resonances [12].

Available macroscopic-microscopic models essentially differ in the derivation of the macroscopic (LD-like) contribution to the PES, with minor difference in the modeling of the microscopic part. Together with inclusion of deformation [13,14] and rotation [15], developments of the macroscopic term involved higher-order effects in the leptodermous expansion of the nuclear binding energy, such as curvature and Gauss-curvature terms [16–19]. Krappe, Nix, Sierk, and collaborators [20,21] accounted for the finite range of nuclear forces, nuclear saturation, and diffuseness of the surface. That yielded the Finite-Range Liquid Drop Model (FRLDM). In parallel to these developments, the deformation dependence of the so-called Wigner [22] or congruence [14] term[1] was established [22–26].

While existing macroscopic-microscopic models perform comparatively well in describing ground-state masses (on which they have been adjusted to), the PES can sizeably vary from one model to another when moving away from the equilibrium configuration [17,27–29]. Sizeable differences can be observed between theoretical fission barriers, and a large part of these differences can be ascribed to the macroscopic contribution [23,30]. An overview of the achievement of different models in describing ground-state masses is given in Ref. [31], and a comparison of predictions for fission barriers can be found in Refs. [17,32].

As a typical large-scale-amplitude collective motion, fission is an ideal research laboratory for probing the PES. Along the fission process, the nucleus evolves from a mononucleus to the configuration of two separated fragments. While the

*mazurek@ifj.edu.pl

[1]Depending on authors, the term Wigner either refers only to the positive part of the congruence energy [23] or it is equivalent to it [18]. In the former terminology, the congruence energy consists of the Wigner term and an additional $A^0$ constant. In this paper, we use the terms Wigner and congruence for referring to the same contribution to the macroscopic energy.

 

PES plays a driving role in this shape evolution, dynamical effects—by means of inertia, friction, and diffusion forces—are also crucial [33]. If the influence of the PES is sufficiently strong, the difference between PES models may manifest itself in the fission observables. To be most sensitive to the macroscopic part of the PES, fission at high excitation energy is best suited, because microscopic effects are negligible. Restriction to high excitation energies, in addition, allows using simplifying assumptions. While heavy fissioning nuclei hardly deviate from an ellipsoidlike shape, lower-fissility nuclei exhibit shapes which are more deformed: The saddle point of low-fissility systems is very close to scission, resembling two distorted spheroids separated by a well-developed neck. As a consequence, the parametrization of the PES is expected to be more critical for fission of medium-mass nuclei compared to fission of heavy systems. In particular, (i) appropriate modeling of surface *and* curvature effects is important, and (ii) sensitivity to the deformation dependence of the Wigner/congruence energy may be largest. In a previous work [27], we concentrated on the former aspect, with a careful study of the influence of the LD prescription used for the PES on customary fission observables. In the present work, we pursue and deepen our investigation by additionally examining the contribution from the shape-dependent Wigner/congruence energy. As in Ref. [27], we consider fission of a hot and rotating medium-mass compound nucleus. We considerably extend the set of investigated observables and test the sensitivity of usually disregarded quantities. Note that the moderate fissility of medium-mass systems makes the investigation challenging. Three-dimensional Langevin calculations for $^{132}$Ce [34,35] and our previous work on $^{118}$Ba [27], dedicated, respectively, to friction and the "bulk" macroscopic part of the PES, were pioneering in this respect. The present work is a next step in this direction.

The paper is organized as follows. In Sec. II the model is presented with a brief description of the formalism (Sec. II A) and special focus on the ingredients of particular importance for this work (Sec. II B). Results are gathered in Sec. III and compared with experiment wherever available. Section IV discusses the observations in the light of other studies. Concluding remarks are given in Sec. V. Part of the work was presented before in Ref. [36].

## II. DESCRIPTION OF THE MODEL

### A. General framework

A fully microscopic description of fission is challenging [37,38]. The decay of hot rotating compound nuclei can reliably be described by using a transport theory, which distinguishes between collective and intrinsic degrees of freedom (see Refs. [39,40] and references therein). Within Kramers' seminal picture [41], the collective modes can be viewed as Brownian particles interacting stochastically with a heat bath. The evolution of the system is given by solving either the (differential) Fokker-Planck or the (integral) Langevin classical equations of motion. The combined action of driving potential, inertia, friction, and diffusion forces is calculated. It determines the trajectory of the nucleus on the PES. As compared to the Fokker-Plank equation, the Langevin approach permits tracing the evolution of the system step by step in time for individual trajectories. Note, that it can be solved exactly in a multidimensional space [39]. The present work uses the three-dimensional Langevin model developed by Adeev and collaborators [42]. This code has been successful in describing experimental data on heavy-ion fusion-induced fission over a wide range of initial compound nucleus (CN) masses, excitation energies, and angular momenta [34,43–48]. The main features of the model are given below. We refer the reader to the quoted literature for further details.

Within the stochastic approach, the dynamical evolution of the system is obtained by solving the set of coupled Langevin equations:

$$\begin{aligned}\frac{dq_i}{dt} &= \sum_j \mu_{ij}(\vec{q})p_j,\\ \frac{dp_i}{dt} &= -\frac{1}{2}\sum_{j,k}\frac{d\mu_{ij}(\vec{q})}{dq_i}p_j p_k - \frac{dF(\vec{q})}{dq_i}\\ &\quad - \sum_{j,k}\gamma_{ij}(\vec{q})\mu_{ij}(\vec{q})p_k + \sum_j \theta_{ij}(\vec{q})\Gamma_j(t),\end{aligned} \tag{1}$$

where $\vec{\mathbf{q}} = (q_1, q_2, q_3)$ is the vector of collective coordinates and $\vec{\mathbf{p}}$ the corresponding conjugate momentum. The collective coordinates are closely related to the choice of the parametrization of the nuclear shape. In the present model, they are based [42,45] on the Funny Hills $(c, h, \alpha)$ parametrization [49]. The variables $(q_1, q_2, q_3)$ are connected to elongation, neck thickness and mass asymmetry of the nucleus, respectively. The driving potential is given by the Helmholtz free energy $F(\vec{q}) = V(\vec{q}) - a(\vec{q})T^2$, where $V(\vec{q})$ is the bare potential energy (see Sec. II B). A Fermi-gas model is used for the determination of the temperature according to $T = \sqrt{E_{\rm int}/a}$, where $E_{\rm int}$ and $a$ are the intrinsic excitation energy and level-density parameter, respectively. Several options are implemented in the code for the latter [50]. We assume in this work a constant value for $a$, as we observed that it has no influence on the conclusions of this study. The mass tensor $m_{ij}(\vec{q})$ ($\|m_{ij}\| = \|\mu_{ij}\|^{-1}$) is calculated based on the Werner-Wheeler approximation for incompressible irrotational flow [51]. The friction tensor $\gamma_{ij}(\vec{q})$ is derived within the *wall-and-window* one-body dissipation mechanism [52] with a reduced strength of the contribution from the *wall* by means of a factor denoted $k_s$ [43,44]. Indeed, it has been established that the original derivation of the *wall-and-window* friction model predicts too-strong friction [53–56] and that $k_s < 1$ is necessary to reproduce experimental data consistently [42,44,57]. The last term on the right-hand side of Eq. (1) is related to the diffusion tensor $D_{ij}(\vec{q}) = \theta_{ik}\theta_{kj}$ derived from Einstein's relation: $D_{ij}(\vec{q}) = \gamma_{ij}(\vec{q})T$, where $\theta_{ik}$ is the random force strength tensor. The stochastic nature of the diffusion process is accounted for by the normalized Gaussian white noise term $\Gamma_j(t)$.

The initial conditions of the system are assumed to correspond to a spherical CN with a total excitation energy $E^\star$ given by the entrance channel of the reaction. The angular momentum $L$ for each Langevin trajectory is sampled from a

triangular distribution with a maximum given by the critical angular momentum $L_{\max}$ for fusion [40]. The initial conditions in the $\vec{\mathbf{p}}$ momentum assume thermal equilibrium [43].

Deexcitation of the system by evaporation of light particles $(n, p, \alpha)$ is taken into account along the path to scission using the Monte Carlo approach [40,58]. The decay width for the emission of a given particle is calculated with an updated version of the statistical code LILITA [59] based on Hauser-Feschbach theory [6]. In this calculation, the level-density parameter $a$ is assumed to be constant, as mentioned above. Transmission coefficients are derived from fusion systematics [60]. A sharp rigid sphere prescription with a radius parameter $r_0 = 1.2$ fm is used for the yrast line. Although barriers for charged-particle emission can be made deformation dependent in the model [34,42], they are calculated for a spherical shape in this work. For the systems studied here, this simplification affects mainly particle-energy spectra, which we do not consider, and only to minor extent particle multiplicities, which are the focus in our study. In contrast to Ref. [27], deexcitation of the fission fragments after scission is explicitly included. That makes it possible to evaluate the relevance of some more observables. Postscission light-particle emission is computed in a way similar to prescission evaporation.

During a random trajectory walk in the collective coordinate space, energy conservation is ensured according to $E^\star = E_{\text{int}} + E_{\text{coll}} + V(\vec{q}) + E_{\text{evap}}(t)$, where $E_{\text{coll}}$ is the kinetic energy of the collective motion, and $V(\vec{q})$ is the potential energy at the actual point on the PES of the trajectory at time $t$. Both implicitly depend on the angular momentum by including the rotational energy. The energy carried away by particle evaporation at time $t$ is accounted for by $E_{\text{evap}}(t)$. Note that, to limit computing time, each trajectory is simulated dynamically for a finite period of time only, and the transition to a statistical branch is implemented under appropriate conditions [40]. In the statistical branch, the fission-decay width is calculated using the generalized Kramers' formula in the multidimensional space [61]. This formula accounts for the value of the potential energy, mass, and friction tensors near the ground state and near the saddle point. It provides a very reasonable representation of a more elaborate calculation for medium-mass nuclei, which have high fission barriers $B_f$ and for which the fission-decay width is mainly determined by the factor $\exp(-B_f/T)$. If the nucleus is committed to fission, the code switches again to the dynamical Langevin treatment for completing the trajectory beyond saddle. Scission is defined by the criterion of a finite neck radius $R_N = 0.3R_0$, with $R_0$ as the radius of the corresponding CN [62]. At scission, the excitation energy is shared among the two fragments according to their mass ratio.

### B. Potential energy surface and deformation-dependent Wigner/congruence term

A crucial ingredient of the Langevin equations is the PES $V(\vec{q})$. It appears in the driving term $dF(\vec{q})/dq_i$ in Eq. (1), and it enters the equation ensuring energy conservation. As in Ref. [27], we consider two LD variants for the PES: FRLDM [20–22,25] and the Lublin-Strasbourg-Drop (LSD) model [17,26,63], which are representative examples describing experimental masses and fission barriers with good precision. A unique feature of FRLDM is the proper account of the diffuseness of the nuclear surface, and corresponding deformation-dependent nuclear, rotational, and Coulomb contributions [20,64]. The LSD prescription [17] was derived from the original LD formula. Its key feature is a deformation-dependent curvature energy term which is added to the deformation-dependent surface, rotational, and Coulomb terms. We have previously shown [27] that the respective specificities of FRLDM and LSD can yield strikingly different PESs for medium-mass nuclei and, consequently, different fission-fragment mass $A$, charge $Z$, and total kinetic energy TKE distributions. In both models, taking an additional deformation-dependent Wigner (FRLDM) Wigner/congruence (LSD) term into account has shown to improve the description of fission barriers considerably [25,26,65]. The present work investigates the influence of the PES in detail, by comparing dynamical calculations obtained without and with a deformation-dependent Wigner/congruence contribution.

The necessity for a Wigner/congruence term was revealed in the "V-shaped" systematics of nuclear masses [14]. Although a connection has been made with quantization in a finite potential well [66], it became customary to model the V shape phenomenologically in the macroscopic contribution to the binding energy. Furthermore, it is well established that the Wigner/congruence term must depend on deformation: When a nucleus moves towards fission, the Wigner/congruence energy of both fragments has to emerge progressively, i.e., it has to double at scission. Because medium-mass nuclei have strongly necked-in saddle-point shapes, the introduction of a deformation-dependent Wigner/congruence energy affects the height of the fission barrier substantially. In contrast, for heavy systems, the saddle-to-scission path is longer, and the aforementioned doubling at scission of the Wigner/congruence term hardly affects the barrier.

To examine possible signatures of the deformation-dependent Wigner/congruence energy in fission dynamics, the study considers a set of four PESs, involving two LD variants and their respective deformation-dependent Wigner/congruence energy:

(i) FRLDM [21] without deformation-dependent Wigner term;
(ii) FRLDM [25] with deformation-dependent Wigner term;
(iii) LSD [17] without deformation-dependent congruence term;
(iv) LSD [26] with deformation-dependent congruence term.

The deformation dependence of the Wigner/congruence energy has to set in when the nucleus develops a neck, and it has to reach full strength at scission. Yet, the best-suited parametrization is still debated [18,22,24,25,29]. To guide understanding of the results, we remind the reader here below of the formulas used in FRLDM and LSD.

The modeling of the deformation dependence of the Wigner energy within FRDLM used in the present work is given by

the following updated prescription [67]:

$$E^{\mathrm{FRLDM}}_{\mathrm{Wign}}(\vec{q}) = \left[W^{\mathrm{FRLDM}}_0(I) + a_0 A^0\right] B_{\mathrm{Wign}}(\vec{q}), \tag{2}$$

$$B_{\mathrm{Wign}}(\vec{q}) = \begin{cases} \left[1 - \left(\frac{R_{\mathrm{neck}}(\vec{q})}{R_{\mathrm{frag}}(\vec{q})}\right)^2\right]^2 + 1, & \text{necked-in shapes,} \\ 1, & \text{otherwise,} \end{cases} \tag{3}$$

$$W^{\mathrm{FRLDM}}_0(I) = \begin{cases} W_1 \cdot |I| \cdot \left(1 - \frac{C_1}{C_2}|I|\right), & |I| \leqslant 0.35, \\ W_1 \cdot C_1 \cdot C_2, & |I| > 0.35, \end{cases} \tag{4}$$

where $I = (N - Z)/A$, $a_0 = 2.615$ MeV, $W_1 = 38.38$ MeV, $C_1 = 0.5$, and $C_2 = 0.35$. The deformation dependence is determined by the radius $R_{\mathrm{neck}}(\vec{q})$ of the neck and the radius $R_{\mathrm{frag}}(\vec{q})$ of the nascent light fission fragment. For nuclei with $100 \leqslant A \leqslant 250$, Eqs. (2) and (3) yield results very close to the original prescription of Refs. [22,64].

In the calculations with LSD, the deformation-dependent congruence term is parametrized according to [26,66]

$$E^{\mathrm{LSD}}_{\mathrm{cong}}(\vec{q}) = W^{\mathrm{LSD}}_0(I) B_{\mathrm{cong}}(\vec{q}), \tag{5}$$

$$B_{\mathrm{cong}}(\vec{q}) = \begin{cases} \left(2 - \frac{R_{\mathrm{neck}}(\vec{q})}{R_{\mathrm{frag}}(\vec{q})}\right), & \text{necked-in shapes,} \\ 1, \text{otherwise,} \end{cases} \tag{6}$$

$$W^{\mathrm{LSD}}_0(I) = -C_3 \exp(-W_2|I|/C_3), \tag{7}$$

where $C_3 = 10$ MeV and $W_2 = 42$ MeV. In Eq. (6), while $R_{\mathrm{neck}}(\vec{q})$ has the same definition as in Eq. (3), the radius $R_{\mathrm{frag}}(\vec{q})$ was originally defined [66] as the mean of the effective transverse radii of the two nascent fragments. This prescription leads to a quite abrupt change in the congruence energy when the neck appears. Thus, in the present work, $R_{\mathrm{frag}}(\vec{q})$ is taken as the radius of the nascent light fission fragment, analog to the FRLDM prescription. That modifies the original prescription of Refs. [26,66] only weakly, while it makes the deformation-dependent contribution to the energy more smooth in the transition region between ellipsoidlike and necked-in shapes.

The PES for an $^{111}$In CN, as calculated with FRLDM including the deformation-dependent Wigner energy, is displayed in Fig. 1 in the two-dimensional ($q_1$, $q_3$) subspace, assuming $h = 0$ along the bottom of the fission valley [49]. To start with, we consider a nonrotating ($L = 0\hbar$) system. The total macroscopic energy is shown in the top panel, while the modification of the landscape caused solely by deformation dependence of the Wigner energy is given in the bottom panel: To highlight the influence of the deformation dependence, the constant value of the Wigner energy before necking sets in (i.e., obtained for $B_{\mathrm{Wign}} = 1$) has been subtracted. Similarly, Fig. 2 displays the total LSD macroscopic energy (top), and the deformation-dependent part of the congruence energy (bottom). The deformation-dependence of the Wigner/congruence energy influences the topography of the PES after appearance of a neck at $q_1 > (1.6$–$1.75)$ (the exact value depending on $q_3$). As anticipated from Eqs. (4)–(7), the deformation-dependent parts of the Wigner (FRLDM) and congruence (LSD) terms are of opposite sign, but of similar absolute magnitude. Their dependencies on elongation and asymmetry are very similar too. The total macroscopic energy (top panels of Figs. 1 and 2) exhibits a very different pattern for FRLDM and LSD. The

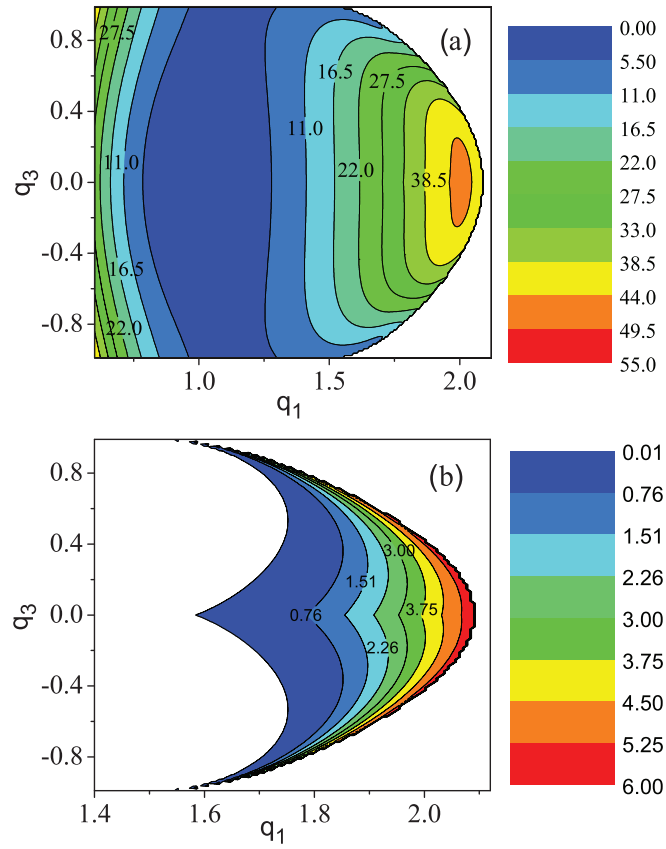


FIG. 1. (Color online) Two-dimensional ($q_1, q_3$) PES for the $^{111}$In nucleus assuming $h = 0$ and $L = 0\hbar$ calculated within FRLDM. The total macroscopic energy and the deformation-dependent part of the Wigner energy [see Eq. (2)] are shown in the top and bottom panel, respectively.

fission barrier and the stiffness of the PES with respect to the asymmetry degree of freedom are larger with LSD. As shown in Ref. [27], this difference is caused by the bulk part of the LD variant. The magnitude and dependence of the Wigner/congruence energy on deformation modifies the PES substantially, but the influence *reduces* the difference between the FRLDM and LSD landscapes. This is better illustrated in Fig. 3, where the one-dimensional symmetric fission path (setting $h = \alpha = 0$) is shown, as obtained with the four PES variants for nonrotating $^{111}$In (top) and $^{229}$Np (bottom) compound nuclei. Each curve was normalized to the energy of the corresponding spherical ground-state minimum to highlight deformation effects. Inclusion of a shape-dependent Wigner energy in FRLDM increases the height of the fission barrier. In contrast, the shape-dependent congruence energy decreases the barrier for LSD. All in all, the difference between the bulk part of the two LD prescriptions gets reduced. It is worth noting that the magnitude of this compensation depends on the system: The effect is seen to be large (negligible) for $^{111}$In ($^{229}$Np). That is attributed to the degree of deformation and necking of the corresponding saddle-point shape. For heavy systems, the influence of the Wigner/congruence term is limited to the saddle-to-scission path and, namely, to the slope of the descent; see Fig. 3 (bottom).

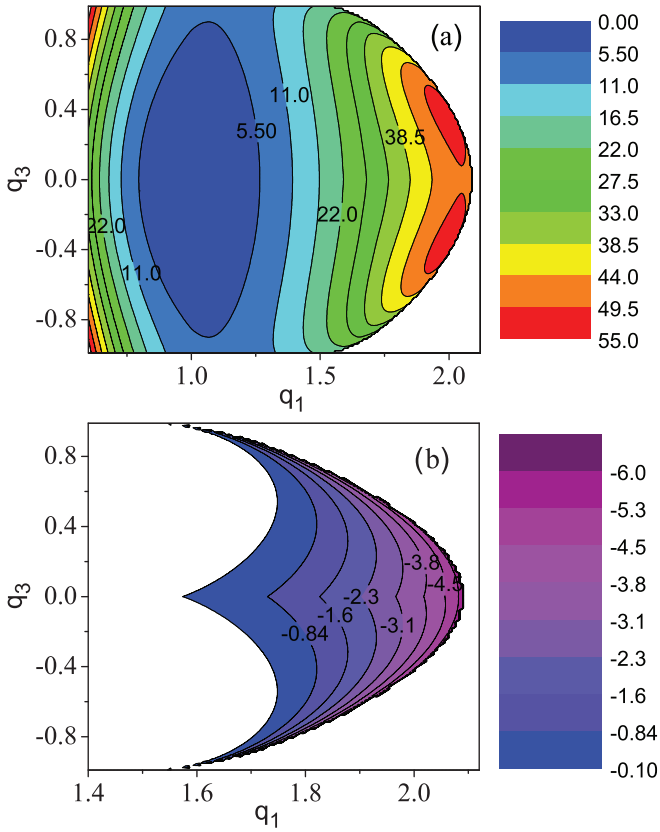


FIG. 2. (Color online) Two-dimensional $(q_1, q_3)$ PES for the $^{111}$In nucleus assuming $h = 0$ and $L = 0\hbar$, calculated within LSD. The total macroscopic energy and the deformation-dependent part of the congruence energy [see Eq. (5)] are shown in the top and bottom panel, respectively.

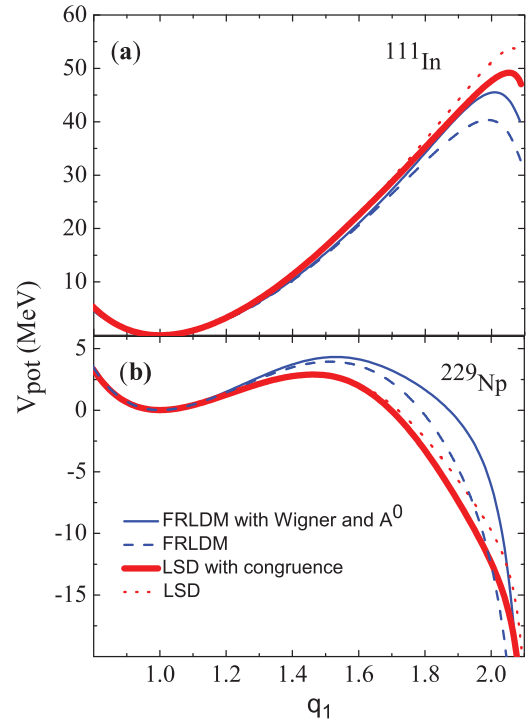


FIG. 3. (Color online) One-dimensional fission path as a function of $q_1$ for nonrotating ($L = 0\hbar$) compound nuclei $^{111}$In (top) and $^{229}$Np (bottom). Both $h$ and $\alpha$ have been set to 0 as a good approximation for the bottom of the fission valley at high excitation energies. Four PES prescriptions are shown: FRLDM without deformation-dependent Wigner term (thin dashed blue line), FRLDM with deformation-dependent Wigner term (thin full blue line), LSD without deformation-dependent congruence term (thick dotted red line), and LSD with deformation-dependent congruence term (thick full red line).

## III. RESULTS

The chosen variant of the LD model and the accurate account of a deformation-dependent Wigner/congruence term defines the topography of the potential energy landscape. The fission probability depends primarily on the height of the barrier, while the properties ($A$, $Z$, TKE) of the fission fragments are mostly determined by the stiffness of the PES between saddle and scission. Prescission light-particle multiplicities depend on the time scale of the process, as governed by the dynamical evolution on the potential landscape. According to the dependence of the Wigner/congruence term on the elongation and asymmetry coordinate, all these observables are expected to be sensitive to details of the PES. To enhance this sensitivity, for reasons argued above, we consider a medium-mass fissioning nucleus. The aforementioned study on $^{132}$Ce [34,35] focused on the investigation of nuclear viscosity and overlooked the influence of the PES prescription. The study used observables connected to both the fission and the evaporation-residue (ER) channels. Our work on $^{118}$Ba in Ref. [27] concentrated on the influence of the bulk part of the PES by probing surface and curvature effects. It was restricted to the analysis of fission observables. The present study performs an analysis of a wide set of observables in both the fission and the ER channels, for hot and rotating $^{111}$In compound nuclei. In addition to conventional observables, we investigate if isotopic and isobaric distributions of fission and ER products can reveal PES effects. Experimental data are available for the reaction $^{84}$Kr + $^{27}$Al measured at two bombarding energies, 5.9 MeV/nucleon [68] and 10.6 MeV/nucleon [69], populating $^{111}$In at an excitation energy $E^*$ of 110 and 205 MeV, respectively. Tables I and II summarize the results for several observables at the low and high bombarding energy, respectively. Figures 4 and 6–8 display integral mass and charge, as well as isobaric and isotopic distributions for either the fission or the ER channel. The calculations presented in this paper assume a reduction factor of the one-body dissipation strength $k_s = 0.6$ and a level-density parameter $a = A/10$. The maximum angular momentum $L_{max}$ of the initial CN is taken as recommended in the experimental analysis [68,69], i.e., $69\hbar$ and $85\hbar$ at 5.9 and 10.6 MeV/nucleon, respectively. These values are consistent with the prescription of Refs. [40,70]. No attempt was made to adjust the model parameters and to achieve best agreement with experiment. Rather, the focus is on searching for signatures of PES details. Nevertheless, because some observables are very sensitive to the model ingredients, we have checked that the conclusions of this work remain unaltered, independent of the actual value of adjustable parameters.

TABLE I. Calculated results for $^{84}$Kr (5.9 MeV/nucleon) + $^{27}$Al leading to hot rotating $^{111}$In CN. The different rows correspond to fission probability $P_f$; prescission neutron $n_{\rm pre}$, proton $p_{\rm pre}$, and $\alpha$-particle $\alpha_{\rm pre}$ multiplicities; postscission neutron $n_{\rm post}$, proton $p_{\rm post}$, and $\alpha$-particle $\alpha_{\rm post}$ multiplicities; neutron $n_{\rm ER}$, proton $p_{\rm ER}$, and $\alpha$-particle $\alpha_{\rm ER}$ multiplicities in the ER channel; mean fission-fragment total kinetic energy $\langle$TKE$\rangle$; variance of the fission-fragment charge $\sigma_Z$ and total kinetic energy $\sigma_{\rm TKE}$ distributions; and mean excitation energy $\langle E^*_{\rm sc}\rangle$ of the fission-fragment pair at scission. Different columns correspond to various prescriptions for the PES (FRLDM and LSD without and with Wigner/congruence term) and experiment wherever available. To restrict to ER or fission-fragment products, the calculated events were filtered, considering masses larger than 15 only; see Fig. 4 (left panel).

| | FRLDM | | LSD | | Experiment |
|---|---|---|---|---|---|
| | No Wigner | Wigner | No congruence | Congruence | [68] |
| $P_f$ | 0.17 | 0.14 | 0.08 | 0.17 | $0.16 \pm 0.04$ |
| $n_{\rm pre}$ | 0.45 | 0.51 | 0.36 | 0.35 | |
| $n_{\rm post}$ | 0.46 | 0.49 | 0.97 | 0.89 | |
| $n_{\rm ER}$ | 4.36 | 4.31 | 4.13 | 4.25 | |
| $p_{\rm pre}$ | 0.05 | 0.02 | 0.02 | 0.02 | |
| $p_{\rm post}$ | 0.03 | 0.03 | 0.04 | 0.04 | |
| $p_{\rm ER}$ | 0.51 | 0.49 | 0.47 | 0.49 | |
| $\alpha_{\rm pre}$ | 0.01 | 0.00 | 0.00 | 0.00 | |
| $\alpha_{\rm post}$ | 0.05 | 0.04 | 0.14 | 0.12 | |
| $\alpha_{\rm ER}$ | 0.53 | 0.53 | 0.51 | 0.52 | |
| $\sigma_Z$ (amu) | 8.72 | 8.81 | 4.97 | 5.12 | |
| $\langle$TKE$\rangle$ (MeV) | 72 | 70.12 | 79.43 | 80.36 | |
| $\sigma_{\rm TKE}$ (MeV) | 8.77 | 8.87 | 4.83 | 5.34 | |
| $\langle E^*_{\rm sc}\rangle$ (MeV) | 58.19 | 59.56 | 75.30 | 72.29 | |

Before discussing the theoretical results, a word of caution is appropriate concerning comparison with the measurements. At 5.9 MeV/nucleon bombarding energy, fusion-evaporation and fusion-fission dominate the reaction cross section. It is thus legitimate to compare the calculated ER mass and charge distributions with those measured by Schneider *et al.* [68]. At 10.6 MeV/nucleon bombarding energy, mechanisms which are *not* modeled in the present approach contribute to the measured production. According to the systematics of Morgenstern *et al.* [71], incomplete fusion is expected to account for at least 25% of the total (complete + incomplete) fusion cross section at 10.6 MeV/nucleon (this contribution is estimated to be less than 5% at 5.9 MeV/nucleon). The observables measured in Ref. [69] do not permit discriminating complete from incomplete fusion. Also, the maximum value of the angular momentum induced into the system [70] at 10.6 MeV/nucleon exceeds the value of $L$ for which the CN fission barrier vanishes [21], suggesting the presence of a fast-fission component. Last, heavy and intermediate-mass fragments can

TABLE II. Identical to Table I for $^{84}$Kr (10.6 MeV/nucleon) + $^{27}$Al, except that $n_{\rm ER}$, $p_{\rm ER}$, and $\alpha_{\rm ER}$ are not given owing to their weak sensitivity to the PES assumptions; see text. To restrict to ER or fission-fragment products, the calculated events were filtered, considering masses larger than 25 only; see Fig. 4 (right panel). A larger mass cutoff filter is used as compared to Table I to limit the contribution of mechanisms that are not modeled. Note that, owing to this filtering, the numerical values of $\sigma_Z$ given for FRLDM are smaller than what the corresponding curves in Fig. 4 show. The quoted $\sigma_Z$'s restrict to the symmetric region, excluding the tails of the asymmetric peaks, which—together with the symmetric component—lead to a nearly flat distribution.

| | FRLDM | | LSD | | Experiment |
|---|---|---|---|---|---|
| | No Wigner | Wigner | No congruence | Congruence | [69] |
| $P_f$ | 0.13 | 0.13 | 0.15 | 0.18 | $0.48 \pm 0.07$ |
| $n_{\rm pre}$ | 2.81 | 2.52 | 2.57 | 2.38 | |
| $n_{\rm post}$ | 0.82 | 0.88 | 1.29 | 1.18 | |
| $p_{\rm pre}$ | 0.70 | 0.58 | 0.55 | 0.50 | $1.3 \pm 0.2$ |
| $p_{\rm post}$ | 0.13 | 0.16 | 0.17 | 0.14 | $0.2 \pm 0.1$ |
| $\alpha_{\rm pre}$ | 0.68 | 0.52 | 0.61 | 0.58 | $0.7 \pm 0.4$ |
| $\alpha_{\rm post}$ | 0.22 | 0.30 | 0.57 | 0.59 | $0.3 \pm 0.2$ |
| $\sigma_Z$ | 5.98 | 6.77 | 5.36 | 5.43 | |
| $\langle$TKE$\rangle$ | 80 | 77.4 | 81.4 | 84.6 | |
| $\sigma_{\rm TKE}$ | 9.37 | 9.48 | 8.47 | 7.19 | |
| $\langle E^*_{\rm sc}\rangle$ (MeV) | 79.84 | 92.53 | 95.43 | 100.24 | 68.5–86 |

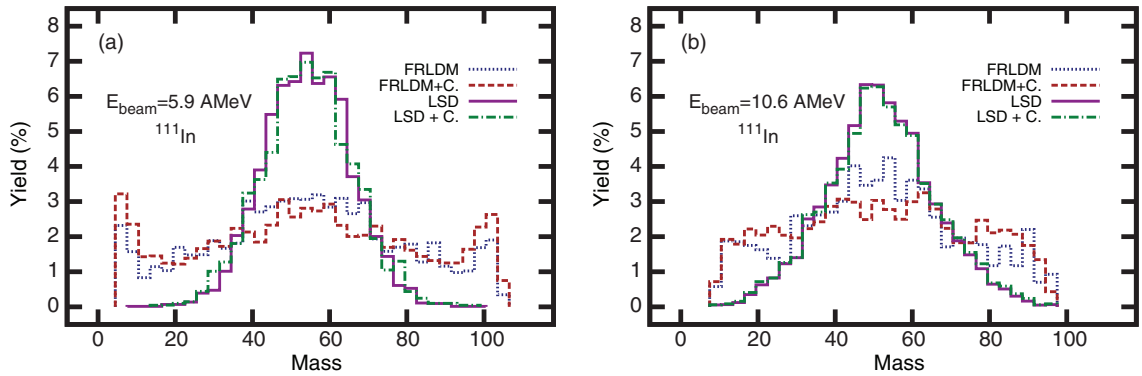


FIG. 4. (Color online) Calculated fission-fragment mass-yield distribution for the reaction $^{84}\mathrm{Kr} + ^{27}\mathrm{Al}$ at 5.9 MeV/nucleon (left) and 10.6 MeV/nucleon (right) bombarding energy, as obtained for various PES variants: FRLDM without (blue dotted line) and with (red dashed line) deformation-dependent Wigner term; LSD without (pink full line) and with (green dash-dotted line) deformation-dependent congruence term.

originate from secondary decays at this excitation energy. A compilation of complementary experiments [72–74] suggests a highly probable contribution of numerous mechanisms in the data set of Ref. [69]. Binary products referred to as fission fragments might thus be of various origins, including fission after complete and incomplete fusion, fast fission, as well as complex primary and secondary heavy and intermediate-mass fragment emission. Because the present model is intended to describe "standard" evaporation and fission after complete fusion, its predictions can be compared to the data of Futami *et al*. [69] to some extent only.

### A. Integral cross sections, light-particle multiplicities, and fission-fragment properties

Table I shows that, for the 5.9 MeV/nucleon experiment, light-particle multiplicities in the ER channel are only weakly sensitive to the bulk part of the macroscopic energy and to the Wigner/congruence term. A similar observation is made at 10.6 MeV/nucleon, and these quantities are not given in Table II. This insensitivity is attributable to the primary dependence of $n_{\mathrm{ER}}$, $p_{\mathrm{ER}}$, and $\alpha_{\mathrm{ER}}$ on the landscape around the compact equilibrium shape, where the different models predict a similar PES topography. In contrast, a strong influence of the bulk part of the LD potential, and of the Wigner/congruence contribution, is observed for the fission probability at the lowest bombarding energy. The difference between the two LSD calculations follows from Fig. 3(a): The decrease of the barrier height with the inclusion of the congruence term leads to an increase of $P_f$ at both bombarding energies. The situation is slightly more puzzling for FRLDM. Indeed, in this case the influence of the Wigner term on the barrier height is not reflected in $P_f$ as a function of the bombarding energy: At 5.9 MeV/nucleon projectile energy, the increased barrier with the Wigner term yields a lower fission probability, while the fission probability is unchanged at 10.6 MeV/nucleon. This is explained by the asymmetry dependence of the Wigner energy. As seen in Fig. 1(b), the latter leads to a larger increase of the barrier for symmetric rather than for asymmetric fission. This feature, combined with the soft FRLDM landscape, allows the fissioning nucleus to bypass the symmetric hill and to overcome the saddle ridge preferentially at nonzero asymmetries, leading to a similar $P_f$ with and without the Wigner term. In addition, the asymmetric trajectories for FRLDM with Wigner term reach scission faster than for FRLDM without Wigner term, yielding smaller prescission multiplicities, a higher fission-fragment excitation at scission, and thus larger postscission multiplicities and lower ⟨TKE⟩; see Table II. Such a bypass of symmetric fission does not occur for LSD, owing to the stiffer PES in the asymmetry-coordinate direction. Consequently, a correlation between the observables as noted above for the two FRLDM calculations is not obtained between the two LSD variants. We note that, by including the Wigner/congruence term, the fission probabilities for FRLDM and LSD get close, in accordance with the similar barrier heights. The calculated fission cross section at 5.9 MeV/nucleon, $\sigma_{\mathrm{fiss}}^{\mathrm{calc}} = 181$ mb for FRLDM and 220 mb for LSD, is in good agreement with the experimental value $\sigma_{\mathrm{fiss}}^{\mathrm{exp}} = 200 \pm 50$ mb. At 10.6 MeV/nucleon, the cross section referred to as fusion-fission by Futami *et al*. [69] includes all binary events with fragment charges $Z \geqslant 5$ and amounts to $\sigma_{\mathrm{fiss}}^{\mathrm{exp}} = 500 \pm 50$ mb. We have obtained a calculated value that is a factor of two smaller. The discrepancy is connected to the contribution of various binary-decay mechanisms in experiment and which are not treated in the model.

Prescission light-particle multiplicities are observed to be most sensitive to the bulk part of the LD prescription and only weakly dependent on details of the PES such as the Wigner/congruence energy. As Fig. 3(a) shows, the four LD variants correspond to barriers differing by a comparable amount of a few MeV. Thus, the stronger influence of the bulk part of the LD energy suggests that prescission multiplicities are mostly emitted prior to the climb to the saddle point, where the deformation-dependent Wigner/congruence term is not yet effective. In spite of the visible dependence of ($n_{\mathrm{pre}}$, $p_{\mathrm{pre}}$, $\alpha_{\mathrm{pre}}$) on the LD variant, the influence of the PES on evaporation prior to scission does not exceed 15%–20% [27]. This limited sensitivity is in contrast with the influence of the PES on postscission evaporation. Tables I and II show that,

while the influence of the Wigner/congruence term remains modest, as in the case of prescission particles, the influence of the bulk part of the LD model is large (up to a factor of 2 difference between FRLDM and LSD). Postscission evaporation depends on the dynamical evolution prior to scission. The latter yields a different excitation energy which is available for the fragments (see last row of Tables I and II) and, thus, different postscission multiplicities. Excitation energy at scission $\langle E^*_{\rm sc}\rangle$ depends on the actual trajectory on the PES on the balance between the potential, collective, and intrinsic energies and the energy carried away by prescission evaporation. Collective and intrinsic energies are close for all calculations, and prescission particle multiplicities do not differ much either. At the same time, as seen in Fig. 3(a) the potential energy near scission in the FRLDM and LSD models differs by about 20 MeV. Consequently, a difference of similar amount is obtained between $\langle E^*_{\rm sc}\rangle$ for the FRLDM and LSD models. Additional account of the Wigner/congruence energy reduces the difference between FRLDM and LSD and, thus, between the excitation energies at scission. In Table II, within the quoted error bars, and bearing in mind that the model does not account for all possible mechanisms, the agreement between calculated and experimental pre- and postscission multiplicities is reasonable.

Figure 4 displays the fission-fragment mass-yield distributions calculated with the four LD variants considered in this work. Because the largest part of the fission cross section is built up by the highest partial waves, complementary to Figs. 1 and 2 for $L = 0\hbar$, we show in Fig. 5 the FRLDM and LSD landscapes for $L = 70\hbar$. It can be seen that the main difference between the two LD prescriptions remains unchanged up to the largest angular momenta involved. The stiff dependence of the LSD potential surface on mass asymmetry, as caused by curvature effects [27], yields a narrow fission-fragment $A$ distribution with a slight broadening for increasing beam energy. In contrast, the soft FRLDM potential landscape leads to wider distributions, and, at the highest bombarding energy, the FRLDM mass distribution is almost flat for $20 \lesssim A \lesssim 80$. This result is typical for systems close to the Businaro-Gallone (BG) point [75,76]. While asymmetric fission fairly competes with symmetric splitting with FRLDM, relatively high hills in the asymmetry-coordinate direction persist for LSD even at $L = 70\hbar$ [see Fig. 5(b)] and confine the fission-fragment distribution around symmetry. The onset (inhibition) of asymmetric fission predicted for $^{111}$In by FRLDM (LSD) is connected to the different location of the BG point, predicted by the two models [27]. The observed difference between mass and charge distributions leads to a similar difference in the TKE distributions, because the latter depend primarily on the product of the fission-fragment $Z$'s at scission. The variances $\sigma_{\rm TKE}$ are observed to be most affected: The large contribution of asymmetric mass splits for FRLDM leads to wider TKE distributions than for LSD. On the contrary, mean $\langle$TKE$\rangle$ values are primarily determined by the product of the fragment charge numbers at symmetry; they are close to each other and in agreement with Viola's systematics [77].

The analysis above, including two LD models without and with their respective Wigner/congruence contribution, does not indicate a clear influence of the parametrization of the deformation-dependent Wigner/congruence energy. In general, the effect does not exceed 10%. The main difference between predictions originates in the prescription used for the bulk part of the LD energy [27]. The sensitivity of the observables, discussed so far, thus remains weak for probing the Wigner/congruence contribution to the PES in fission at high excitation energy. In the next section, the investigation is deepened by considering additional, less conventional, observables.

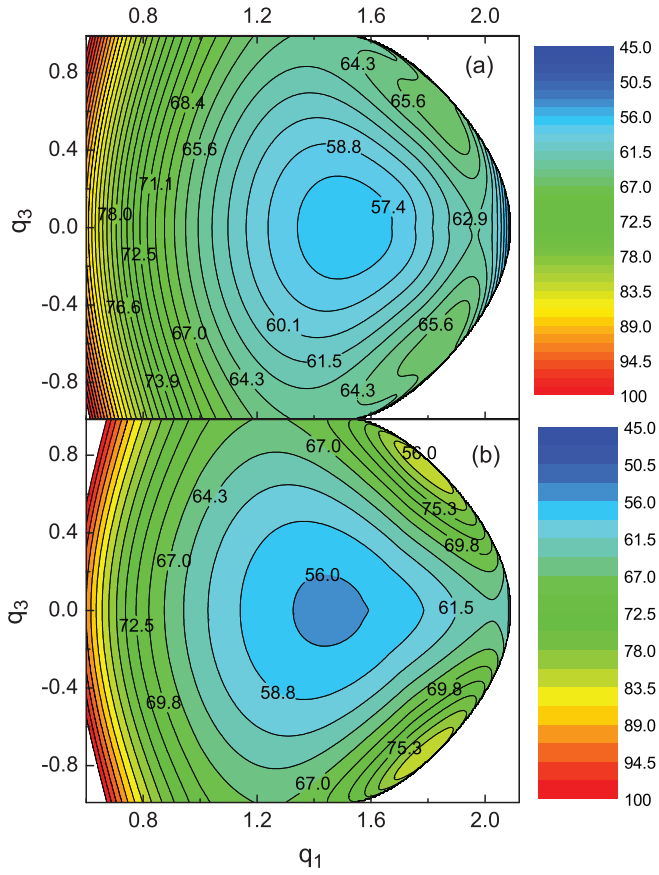


FIG. 5. (Color online) Two-dimensional $(q_1, q_3)$ PES for the $^{111}$In nucleus assuming $h = 0$ and $L = 70\hbar$, calculated within FRLDM with Wigner term (top) and LSD with congruence term (bottom).

### B. Isobaric and isotopic distributions

According to the connection between isospin and Wigner/congruence energy, we investigate the $(A, Z)$ composition of the reaction products in detail.

We start by considering in Fig. 6 the mass and charge content of the ER produced in the reaction $^{84}$Kr(5.9 MeV/nucleon) + $^{27}$Al [68]. The agreement between the measurement and the calculation is rather remarkable, both for the integral and the isobaric distributions. Only a slight overestimation by $\approx$1.5 (0.5) units for the mean ER mass (charge) is noticed. This achievement suggests that the modeling of particle decay widths is reasonable for the present system. The deformation dependence of the transmission coefficients, neglected in the calculation, does not affect evaporation in the ER channel substantially, because the shapes

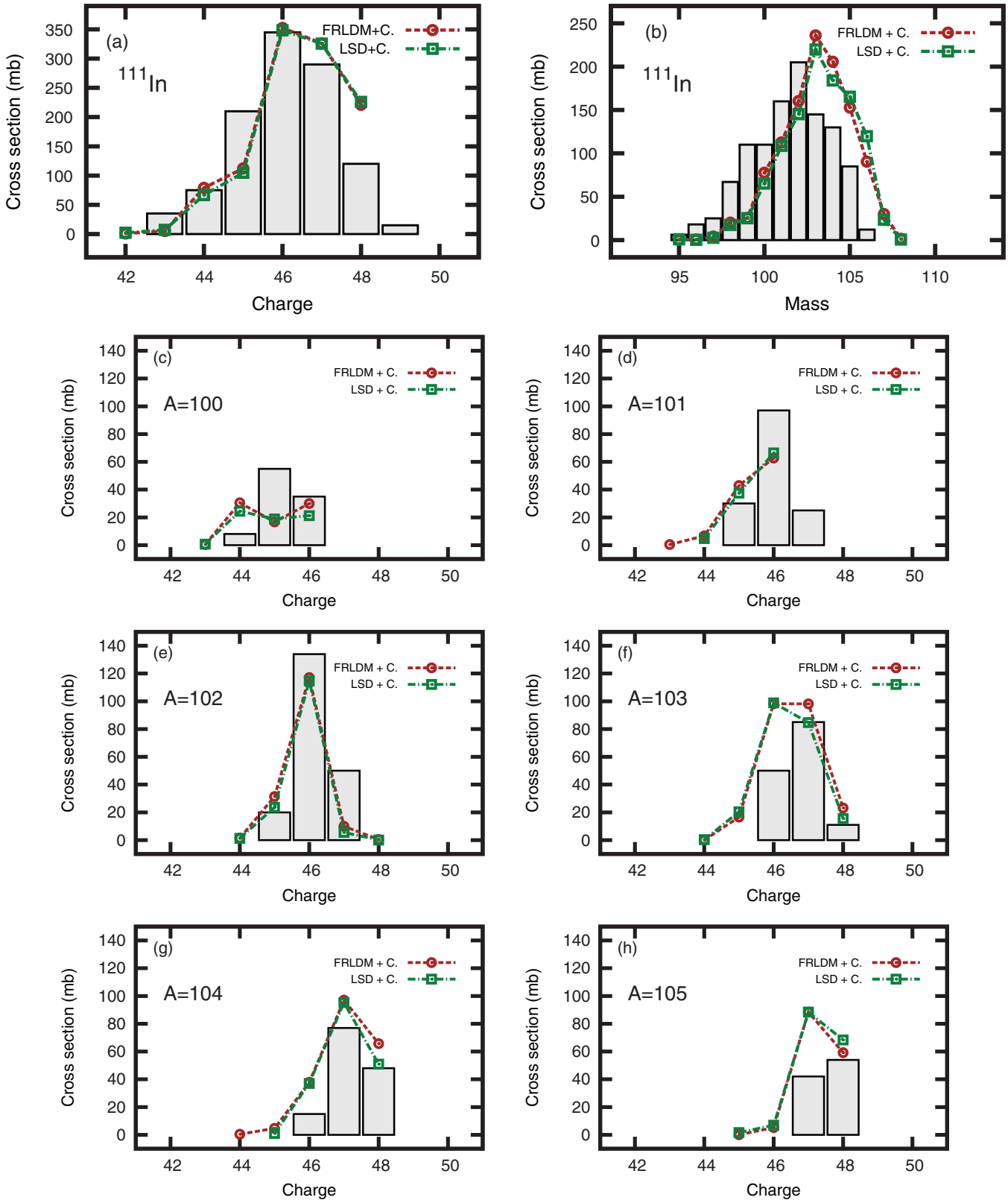


FIG. 6. (Color online) Evaporation-residue cross-section distributions for the reaction $^{84}$Kr + $^{27}$Al at 5.9 MeV/nucleon: Integral (a) charge $Z$ and (b) mass $A$ distributions and isobaric distributions for selected masses: $A = 100, 101, 102, 103, 104, 105$ from (c) to and (h). The data [68] (gray histograms) are compared with predictions of two model variants: FRLDM with deformation-dependent Wigner term (circles joined by dashed red lines) and LSD with deformation-dependent congruence term (squares joined by dash-dotted green lines). Experimental error bars are not shown for clarity; they amount to around 10%–15%.

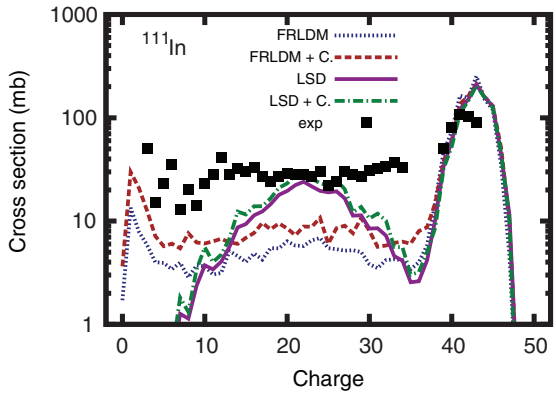


FIG. 7. (Color online) Product charge $Z$ cross-section distribution for the reaction $^{84}\mathrm{Kr} + ^{27}\mathrm{Al}$ at 10.6 MeV/nucleon. The data [69] (black squares) are compared to predictions by various model variants: FRLDM without (blue dotted line) and with (red dashed line) deformation-dependent Wigner term; LSD without (pink full line) and with (green dash-dotted line) deformation-dependent congruence term. Experimental error bars are not shown for clarity.

of the corresponding emitters are predominantly compact. The good agreement between experimental and theoretical absolute cross-section values in Fig. 6 suggests a realistic description of the competition between evaporation and fission at each stage along the deexcitation cascade. We emphasize that isobaric (equivalently, isotopic) ER distributions are poorly studied observables in fusion reactions, owing to the experimental difficulty in identifying heavy products in $(A, Z)$. The data of Schneider *et al.* [68] make it possible to assess a feature of the model presented in Refs. [42–44] that has never been tested. Together with the dedicated work by Adeev and collaborators, Fig. 6 highlights the capabilities of the model to describe various channels and observables. Concerning the search for PES effects, only two calculations are shown in Fig. 6, namely FRLDM with Wigner and LSD with congruence. Corresponding curves without the Wigner/congruence energy would be nearly indistinguishable. Hence, it is observed that, neither the prescription for the bulk part of the LD model nor the parametrization of the Wigner/congruence term has noticeable influence on the ER mass and charge composition. The weak sensitivity is explained by the fact that the topography of the PES affects primarily fissioning trajectories, which explore a more extended region of the landscape, where model prescriptions differ most. The large sensitivity of observables in the fission channel in this respect was already inferred from Fig. 4.

Owing to the weak sensitivity in the ER channel, we turn to fission and compare the calculation with experimental data on $(A, Z)$ of the fragment products measured at 10.6 MeV/nucleon [69]. Figure 7 displays the integral $Z$ distribution, including fusion-evaporation and fusion-fission for the calculation, as well as other possible binary-decay channels for the experiment. The ER component is centered at $Z \approx 42$, evaporated particles are confined to values below $Z = 5$, intermediate-mass fragments likely contribute in the interval $3 \lesssim Z \lesssim 15$, while fission fragments from various compound nuclei (formed in either complete or incomplete fusion) fill in the range $8 \lesssim Z \lesssim 38$. Because the data set collected by Futami *et al.* [69] contains reaction mechanisms which are not described by the present model, the comparison between experiment and predictions can be qualitative, only. Concentrating on the central fission part, two features attract attention. First, the shape of the distribution obtained in calculations with FRLDM resembles the experimental one, but absolute values do not match. The second observation is the close reproduction of the data by LSD calculations around symmetry on an absolute scale. However, the calculated LSD distributions are too narrow to be consistent with experiment. Because the contribution from binary-decay mechanism is different from standard fusion-fission, which mainly populates the asymmetric region, remains unknown, the actual degree of flat character of the fusion-fission component, as suggested by FRLDM, still needs to be confirmed. However, that the rejection of these mechanisms will shrink the experimental distribution to a degree that makes it compatible with LSD seems rather unlikely either. In the absence of further experimental clue, the comparison simply (i) confirms the above-observed negligible deformation-dependent Wigner/congruence effects for the integral mass and charge distributions and (ii) corroborates the conclusion of Ref. [27] on the relevance of fission of medium-mass nuclei, close to the BG point, for discriminating surface and curvature contributions to the macroscopic LD energy.

As a next step in looking for signatures of the deformation-dependent Wigner/congruence energy, measured isotopic distributions for fission-fragment-like products of Ca, K, S, Si, Mg, F, are shown in Fig. 8 and compared with calculations. The model is seen to reasonably describe the mean value and the shape of the isotopic composition for elements near symmetry, such as Ca and K. When moving away from symmetry, the calculated curve gets more and more confined to the neutron-rich side of the distribution and accounts only for part of the isotopes measured. Also, we note that, independent on the element, calculated distributions are too narrow. The observed discrepancy can only partly be ascribed to the negligence of charge fluctuations at scission [78]. The comparison thus supports the likely presence of various binary-decay and secondary-emission fragments in the data set of Ref. [69]. This contribution increases with increasing asymmetry of the partition. Under these circumstances, the agreement of the code with the data close to symmetry is very promising, independent of the used PES variant. A deeper examination of the reliability of the predictions awaits dedicated measurements. Restricting the discussion to the theoretical results, it is noted that for both FRLDM and LSD prescriptions, inclusion of the Wigner/congruence term leads in some cases to an enhancement of the isotopic production on the neutron-deficient side; see, e.g., Si and S. It may be worth studying whether this observation is to be ascribed to the manifestation of a restoring force towards $N = Z$. Furthermore, the detailed survey of theoretical distributions suggests that the Wigner/congruence term may yield a slightly more pronounced local staggering for some elements. In spite of the apparently weak manifestation, these observations may be hints that deserve further investigation. Future studies in this direction should include charge fluctuations [78,79] in the model which will broaden

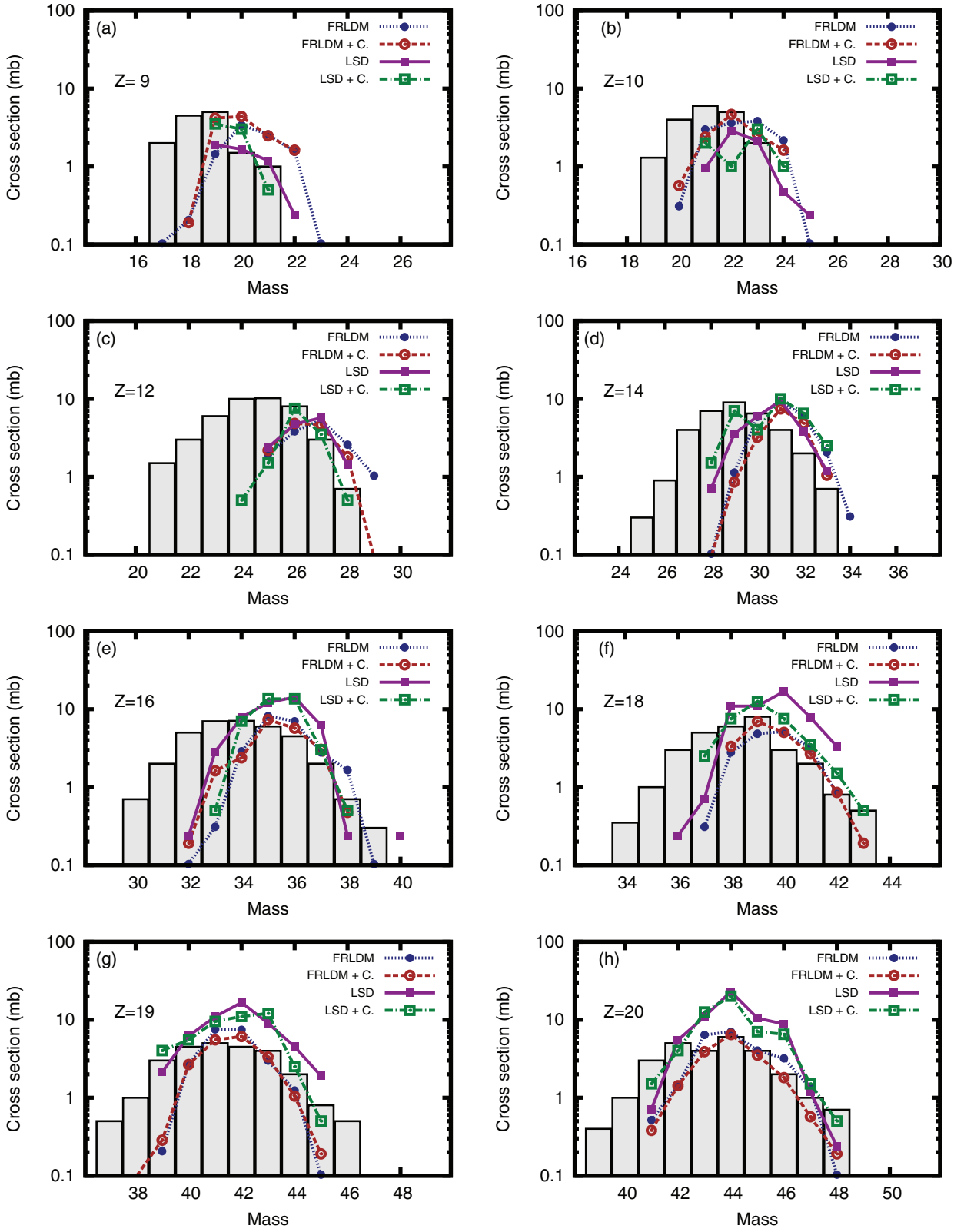


FIG. 8. (Color online) Isotopic cross-section distributions of fission-fragment-like products in the reaction $^{84}$Kr + $^{27}$Al at 10.6 MeV/nucleon for elements of $Z = 9$, 10, 12, 14, 16, 18, 19, 20 from (a) to (h), respectively. The data [69] (gray histograms) are compared to predictions by various model variants: FRLDM without (blue dotted lines) and with (red dashed lines) deformation-dependent Wigner term, LSD without (pink full lines) and with (green dash-dotted lines) deformation-dependent congruence term. Experimental error bars are not shown for clarity; they are below 30% in most cases.

the isotopic distribution of the fission fragment and improve the quantitative comparison with experiment.

## IV. DISCUSSION

The calculations presented in Sec. III confirm the relevance of fission of hot rotating medium-mass nuclei for probing the parametrization of the macroscopic potential energy landscape and, in particular, surface and curvature effects, as we concluded in Ref. [27]. The present study shows, in addition, that the accurate prescription of the deformation-dependence of the Wigner/congruence energy hardly reveals itself unambiguously in high-energy fission. The unusually wide set of observables which we considered leaves this as a challenging task. Interesting differences are nonetheless noticed in the isotopic fission-fragment distributions as calculated without and with the Wigner/congruence term. It remains to be demonstrated that this observation is related to a $N = Z$ driving force. A dedicated study is needed, with inclusion of charge fluctuations on the one hand and further investigation of the best suited initial CN and final product elements on the other hand. That is beyond the scope of the present paper.

Investigations on the influence of the PES parametrization are scarce [27]. Concerning the Wigner/congruence term, most studies focused on static properties [25,26,80], such as ground-state masses and potential energy barriers. Few references attempted to pin down the influence of this specific contribution on the dynamic evolution of the system. To our knowledge, there exists only one investigation studying this aspect: In Ref. [29] Randrup *et al.* employed a dynamical calculation based on the Metropolis method [81] on a five-dimensional PES lattice. They investigated the influence of the shape dependence of the Wigner term on the fragment-mass distribution in low-energy fission of actinides. They found that, if the relatively gentle deformation dependence proposed in Refs. [22,64] is replaced by a more abrupt change near scission, then both the location and the strength of the asymmetric peak in the fission-fragment mass yield for $^{226}$Th are modified significantly. It was nonetheless premature to support a specific prescription for the deformation-dependent Wigner energy, owing to the approximations made for the modeling of other aspects of the approach in Ref. [29]. The apparently discordant conclusion reached in the present work is attributed to the different excitation-energy regime. In low-energy fission of actinides, the location and depth of the fission valleys are of primary importance for determining ($A$, $Z$, TKE) properties of the fragments at scission. The motion may be seen as creeping along the bottom of the valley. The latter is strongly influenced by the neutron and proton composition of the nascent fragments and, thus, by the Wigner/congruence term. On the contrary, in fission at high temperature, dynamics makes the evolution less sensitive to the very bottom profile of the fission path. The stochastic motion leads to numerous random kicks in the momentum space, which smear the influence of the very "floor" of the PES partly out.

In a recent study [82] of binary fragmentation of a compound system $A \approx 60$ at $\approx$8 MeV/nucleon, it was attempted to isolate the influence of a temperature dependence of the Wigner energy. The latter was found to affect mostly the magnitude of the local staggering of the fragmentation, while it did not modify notably the shape and width, i.e., envelope, of the integral product distribution. That is similar to our conclusion for the deformation dependence of the Wigner/congruence energy. Unfortunately, isobaric or isotopic distributions were not studied in Ref. [82].

The statistical model calculations of Mancusi *et al.* [83,84] for the deexcitation of hot compound nuclei, produced either by fusion or spallation, required introducing a constant shift ($\approx$7 MeV) of the emission barriers of heavy-charged products to describe the experiment consistently. This shift was very tentatively (according to the authors of Refs. [83,84]) interpreted as the influence of the Wigner term in the binding energies involved in secondary decays along the deexcitation process, although it was found to be independent of $|N - Z|$, as one would anticipate. The mechanism of standard fusion-fission considered in the present work is less sensitive to similar binding energy considerations, as the corresponding exotic decays are rare in our energy domain. Yet, the observation made in the present work (see Fig. 8) may be worth investigating in connection with the observation by Mancusi *et al.* [83,84].

## V. SUMMARY AND CONCLUSIONS

Among the key aspects affecting the dynamics of fission, the PES of the decaying system is probably the ingredient that attracts less attention in modern dynamical calculations at high temperature. We performed a detailed study of the influence of the potential energy landscape on the decay by fission of hot and rotating $^{111}$In medium-mass nuclei, with the attempt to probe the fine structure of the topography of the landscape. Advanced three-dimensional Langevin calculations were employed, with various descriptions of the LD model and a close attention to the modeling of the deformation-dependent Wigner/congruence energy. More specifically, the FRLDM and LSD descriptions were inserted in the Langevin equation, with their respective parametrization of the Wigner/congruence term. An unusually large set of observables was analyzed, in both the ER and the fission channels, including cross sections, light-particle multiplicities, integral $A$, $Z$, and TKE distributions, as well as isotopic and isobaric distributions of ER and fission-fragment products. Model predictions agree reasonably with available data, emphasizing the power of the approach, and the capabilities of the code used in this work.

Fission-fragment $A$, $Z$, and TKE distributions are found to be most sensitive to the modeling of the potential energy landscape and, in particular, to the treatment of surface and curvature effects. Observables, such as cross sections and light-particle multiplicities, exhibit a lower sensitivity. The study confirms the relevance of fission of hot rotating nuclei close to the BG point for investigating the potential energy landscape. The model-dependence of the latter is rarely tested; the study further suggests the possibility of misinterpreting experimental data by attributing actual PES effects to other fundamental quantities, such as nuclear viscosity and level density, in fission of hot and rotating medium-mass systems.

The present work demonstrates that effects ascribed solely to the deformation dependence of the Wigner/congruence energy are challenging to reveal for customary observables in high-energy fission. Nevertheless, the study also shows that probing the subtle modulation of the potential energy landscape by the deformation-dependent Wigner/congruence term at high temperature merits further investigation. The innovative analysis performed on fission-fragment isotopic distributions, which are expected to be more sensitive to a $|N - Z|$-dependent term, gives hints about the possible evidence of the influence of the deformation-dependent Wigner/congruence energy. The optimum conditions to reveal it unambiguously remain to be accurately determined. Nuclei in the vicinity of the BG point populated at high excitation energy and angular momentum in heavy-ion reactions, supplemented by isotopically resolved measurement of fission fragments, is a very promising tool in this respect. In such sensitive conditions, the observations made along our work may be fully exploited. Constraining the potential energy landscape by means of dynamical calculations would then constitute an alternative and independent way of probing mass models and other fundamental properties of nuclear matter.

## ACKNOWLEDGMENTS

We would like to thank Professor G. D. Adeev and Professor K. Pomorski for stimulating exchange and J. Randrup for useful discussion. Dr. A Heinz is gratefully acknowledged for critical reading of the manuscript and help in formulation. The work was partially sponsored by the French-Polish agreements LEA COPIGAL (Project PARIS) and IN2P3-COPIN (Projects No. 09-136 and No. 12-145), the Polish Ministry of Science and Higher Education (Grant No. 2011/03/B/ST2/01894), and by the Russian RFBR (Project No. 13-02-00168). One of us (P.N.N.) is grateful to GANIL and IFJ PAN for hospitality and financing of his stay at respective laboratory.

[1] S. Aberg, H. Flocard, and W. Nazarewicz, Annu. Rep. Nucl. Part. Sci. **40**, 439 (1990).
[2] J. L. Egido, L. M. Robledo, and R. R. Chasman, Phys. Lett. B **393**, 13 (1997).
[3] J. F. Berger, M. Girod, and D. Gogny, Nucl. Phys. A **502**, 82c (1989).
[4] P. Möller and J. R. Nix, At. Data Nucl. Data Tables **39**, 213 (1988).
[5] H. A. Bethe and R. F. Bacher, Rev. Mod. Phys. **8**, 82 (1936).
[6] C. Weizsäcker, Z. Phys. **96**, 431 (1935).
[7] V. M. Strutinsky, Nucl. Phys. A **95**, 420 (1967); **122**, 1 (1968).
[8] P. Möller, A. J. Sierk, R. Bengtsson, H. Sagawa, and T. Ichikawa, Phys. Rev. Lett. **103**, 212501 (2009).
[9] P. Möller, A. J. Sierk, and A. Iwamoto, Nature (London) **409**, 785 (2001).
[10] P. Jachimowicz, M. Kowal, and J. Skalski, Phys. Rev. C **87**, 044308 (2013), and references therein.
[11] A. Baran, Z. Łojewski, K. Sieja, and M. Kowal, Phys. Rev. C **72**, 044310 (2005).
[12] A. Maj *et al.*, Nucl. Phys. A **731**, 319c (2004).
[13] L. Meitner and O. R. Frisch, Nature (London) **143**, 239 (1939).
[14] W. D. Myers and W. J. Swiatecki, Nucl. Phys. **81**, 1 (1966).
[15] S. Cohen, F. Plasil, and W. J. Świątecki, Ann. Phys. **82**, 557 (1974).
[16] M. Brack, C. Guet, and H.-B. Håkansson, Phys. Rep. **123**, 275 (1985).
[17] K. Pomorski and J. Dudek, Phys. Rev. C **67**, 044316 (2003).
[18] H. J. Krappe and K. Pomorski, *Theory of Nuclear Fission: A Textbook*, Lecture Notes in Physics (Springer, Berlin, 2012).
[19] L. G. Moretto, P. T. Lake, L. Phair, and J. B. Elliott, Phys. Rev. C **86**, 021303(R) (2012).
[20] H. J. Krappe, J. R. Nix, and A. J. Sierk, Phys. Rev. C **20**, 992 (1979).
[21] A. J. Sierk, Phys. Rev. C **33**, 2039 (1986).
[22] P. Möller *et al.*, Nucl. Phys. A **492**, 349 (1989).
[23] W. D. Myers and W. J. Świątecki, Nucl. Phys. A **601**, 141 (1996).
[24] W. D. Myers, *Droplet Model of Atomic Nuclei* (IFI/Plenum, New York, 1977).
[25] P. Möller, A. J. Sierk, and A. Iwamoto, Phys. Rev. Lett. **92**, 072501 (2004).
[26] K. Pomorski and J. Dudek, Int. J. Mod. Phys. E **13**, 107 (2004).
[27] K. Mazurek, C. Schmitt, J. P. Wieleczko, P. N. Nadtochy, and G. Ademard, Phys. Rev. C **84**, 014610 (2011).
[28] J. Randrup and P. Möller, Phys. Rev. Lett. **106**, 132503 (2011).
[29] J. Randrup, P. Möller, and A. J. Sierk, Phys. Rev. C **84**, 034613 (2011).
[30] P. Möller and J. R. Nix, Nucl. Phys. A **229**, 269 (1974).
[31] A. Sobiczewski, and Yu. A. Litvinov, Phys. Scr. T **154**, 014001 (2013).
[32] K. Pomorski, Phys. Scr. T **154**, 014023 (2013).
[33] G. D. Adeev and V. V. Pashkevich, Nucl. Phys. A **405**, 405c (1989), and references therein.
[34] P. N. Nadtochy, A. Brondi, A. Di Nitto, G. La Rana, R. Moro, E. Vardaci, A. Ordine, A. Boiano, M. Cinausero, G. Prete, V. Rizzi, N. Gelli, and F. Lucarelli, EPJ Web Conf. **2**, 08003 (2010).
[35] E. Vardaci *et al.*, AIP Conf. Proc. **1175**, 57 (2009).
[36] K. Mazurek, C. Schmitt, P. N. Nadtochy, A. Maj, P. Wasiak, M. Kmiecik, and B. Wasilewska, Acta Phys. Pol. B **44**, 293 (2013).
[37] V. V. Sargsyan, Yu. V. Palchikov, Z. Kanokov, G. G. Adamian, and N. V. Antonenko, Phys. Rev. A **75**, 062115 (2007).
[38] H. Goutte, J. F. Berger, P. Casoli, and D. Gogny, Phys. Rev. C **71**, 024316 (2005).
[39] Y. Abe, S. Ayik, P.-G. Reinhard, and E. Suraud, Phys. Rep. **275**, 49 (1996).
[40] P. Fröbrich and I. I. Gontchar, Phys. Rep. **292**, 131 (1998).
[41] H. A. Kramers, Physica **7**, 284 (1940).
[42] G. D. Adeev *et al.*, Fiz. Elem. Chastits At. Yadra **36**, 712 (2005) [Phys. Part. Nucl. **36**, 378 (2005)].
[43] A. V. Karpov, P. N. Nadtochy, D. V. Vanin, and G. D. Adeev, Phys. Rev. C **63**, 054610 (2001).
[44] P. N. Nadtochy, G. D. Adeev, and A. V. Karpov, Phys. Rev. C **65**, 064615 (2002).
[45] P. N. Nadtochy and G. D. Adeev, Phys. Rev. C **72**, 054608 (2005).

[46] P. N. Nadtochy, A. V. Karpov, and G. D. Adeev, Yad. Fiz. **65**, 832 (2002) [Phys. At. Nucl. **65**, 799 (2002)].
[47] P. N. Nadtochy, A. V. Karpov, D. V. Vanin, and G. D. Adeev, Yad. Fiz. **66**, 1240 (2003) [Phys. At. Nucl. **66**, 1203 (2003)].
[48] E. G. Ryabov, A. V. Karpov, P. N. Nadtochy, and G. D. Adeev, Phys. Rev. C **78**, 044614 (2008).
[49] M. Brack, J. Damgaard, A. S. Jensen, H. C. Pauli, V. M. Strutinsky, C. Y. Wong *et al.*, Rev. Mod. Phys. **44**, 320 (1972).
[50] A. V. Ignatyuk *et al.*, Yad. Fiz. **21**, 1185 (1975).
[51] K. T. R. Davies, A. J. Sierk, and J. R. Nix, Phys. Rev. C **13**, 2385 (1976).
[52] J. Blocki, Y. Boneh, J. R. Nix, J. Randrup, M. Robel, A. J. Sierk, and W. J. Świątecki, Ann. Phys. (NY) **113**, 330 (1978).
[53] J. R. Nix, and A. J. Sierk, in *Proceedings of the 6th Adriatic Conference on Nuclear Physics: Frontiers of Heavy Ion Physics, Dubrovnik, Yugoslavia, 1987*, edited by N. Cindro, R. Caplar, and W. Greiner (World Scientific, Singapore, 1990), pp. 333–340.
[54] J. R. Nix and A. J. Sierk, in *Proceedings of the International School-Seminar on Heavy Ion Physics, Dubna, USSR, 1986*, edited by M. I. Zarubina and E. V. Ivashkevich (JINR, Dubna, 1987), pp. 453–464.
[55] J. J. Griffin and M. Dworzecka, Nucl. Phys. A **455**, 61 (1986).
[56] S. Pal and T. Mukhopadhyay, Phys. Rev. C **57**, 210 (1998).
[57] P. N. Nadtochy, E. G. Ryabov, A. E. Gegechkori, Yu. A. Anischenko, and G. D. Adeev, Phys. Rev. C **85**, 064619 (2012).
[58] N. D. Mavlitov, P. Fröbrich, and I. I. Gontchar, Z. Phys. A **342**, 195 (1992).
[59] LILITA_N97 is an extensively modified version of the original Lilita program made by J. Gomez del Campo and R. G. Stockstad, Oak Ridge National Laboratory Report No. TM7295, 1981 (unpublished).
[60] L. C. Vaz *et al.*, Z. Phys. A **318**, 231 (1984).
[61] Z. Jing-Shang and H. A. Weidenmüller, Phys. Rev. C **28**, 2190 (1983).
[62] M. V. Borunov, P. N. Nadtochy, G. D. Adeev *et al.*, Nucl. Phys. A **799**, 56 (2008).
[63] J. Dudek, K. Pomorski, N. Schunck, and N. Dubray, Eur. Phys. J. A **20**, 15 (2004).
[64] P. Möller, J. R. Nix, W. D. Myers, and W. J. Świątecki, At. Data Nucl. Data Tables **59**, 185 (1995).
[65] K. Pomorski and F. Ivanyuk, Int. J. Mod. Phys. E **18**, 900 (2009).
[66] W. D. Myers and W. J. Swiatecki, Nucl. Phys. A **612**, 249 (1997).
[67] A. J. Sierk (private communication).
[68] W. F. W. Schneider, F. Pühlhofer, R. P. Chestnut, C. Volant, H. Freiesleben, W. Pfeffer, and B. Kohlmeyer, Nucl. Phys. A **371**, 493 (1981).
[69] Y. Futami *et al.*, Nucl. Phys. A **607**, 85 (1996).
[70] R. Bass *et al.*, Phys. Lett. B **47**, 139 (1973).
[71] H. Morgenstern, W. Bohen, W. Galster, K. Grabisch, and A. Kyanowski, Phys. Rev. Lett. **52**, 1104 (1984).
[72] V. E. Viola, R. G. Clark, W. G. Meyer, A. M. Zebelman, and R. G. Sextro, Nucl. Phys. A **261**, 174 (1976).
[73] Y. Nagame, H. Ikezoe, and T. Ohtsuki, Phys. Rev. C **47**, 1586 (1993).
[74] S. Cavallaro, E. De Filippo, G. Lanzanò, A. Pagano, M. L. Sperduto, R. Dayras, R. Legrain, E. Pollacco, C. Beck, B. Djerroud, R. M. Freeman, F. Haas, A. Hachem, B. Heusch, D. Mahboub, A. Morsad, R. Nouicer, and S. J. Sanders, Phys. Rev. C **57**, 731 (1998).
[75] U. L. Businaro and S. Gallone, Nuovo Cim. **1**, 655 (1925); **1**, 629 (1925).
[76] R. Charity *et al.*, Nucl. Phys. A **483**, 371 (1988).
[77] V. E. Viola, K. Kwiatkowski, and M. Walker, Phys. Rev. C **31**, 1550 (1985).
[78] A. V. Karpov and G. D. Adeev, Eur. Phys. J. A **14**, 169 (2002).
[79] K-.H. Schmidt (private communication).
[80] T. Ichikawa, A. Iwamoto, P. Möller, and A. J. Sierk, Phys. Rev. C **86**, 024610 (2012).
[81] N. Metropolis and S. Ulam, J. Am. Stat. Assoc. **44**, 335 (1949).
[82] C. Karthikraj and M. Balasubramaniam, Phys. Rev. C **87**, 024608 (2013).
[83] D. Mancusi, R. J. Charity, and J. Cugnon, J. Phys. G **420**, 012130 (2013).
[84] D. Mancusi, R. J. Charity, and J. Cugnon, EPJ Web Conf. **17**, 10003 (2011).